A&A 459, 955–963 (2006)
DOI: 10.1051/0004-6361:20054710

Astronomy & Astrophysics

New constrains on Gliese 86 B*

VLT near infrared coronographic imaging survey of planetary hosts

A.-M. Lagrange[1], H. Beust[1], S. Udry[2], G. Chauvin[3], and M. Mayor[2]

[1] Laboratoire d'Astrophysique de Grenoble, Université J. Fourier, BP 53, 38041 Grenoble Cedex 9, France
e-mail: lagrange@obs.ujf-grenoble.fr
[2] Observatoire de Genève, 51 Ch. des Maillettes, 1290 Sauverny, Switzerland
[3] ESO Casilla 19001, Santiago 19, Chile

Received 16 December 2005 / Accepted 1 March 2006

ABSTRACT

Aims. We present the results of multi epoch imaging observations of the companion to the planetary host Gliese 86. Associated with radial velocity measurements, this study aimed at dynamically characterizing with the orbital properties and the mass of this companion (hereafter Gliese 86 B), but also at investigating the possible history of this particular system.
Methods. We used the adaptive optics instrument NACO at the ESO Very Large Telescope to obtain deep coronographic imaging to obtain new photometric and astrometric measurements of Gliese 86 B.
Results. Part of the orbit is resolved. The photometry of Gl 86 B indicates colors compatible with a ~70 Jupiter mass brown dwarf or a white dwarf. Both types of objects fit the available, still limited astrometric data. If we attribute the long term radial velocity residual drift observed for Gl 86 A to B, then the mass of the latter object is $\simeq 0.5\,M_\odot$. We analyse both astrometric and radial velocity data to propose first orbital parameters for Gl 86 B. Assuming Gl 86 B is a $\simeq 0.5\,M_\odot$ white dwarf, we explore the constraints induced by this hypothesis and refine the parameters of the system.

Key words. stars: individual: Gliese 86 – stars: low mass, brown dwarfs – stars: planetary systems – instrumentation: adaptive optics

1. Introduction

One of the biggest challenges of current astronomy is to detect and characterize extrasolar planetary systems, and to understand the way(s) they form and evolve. Over the past decade, technical improvements have allowed detection of more than 150 extrasolar planets via radial velocity (hereafter RV) measurements down to 7.5 Earth Masses (Rivera et al. 2005, minimum mass) around solar type stars, while direct imaging now allows the detection of giant planets around young stars (Lagrange & Moutou 2004; Chauvin et al. 2004). From the theoretical point of view the influence omultiplicity or companionship with outer bodies (e.g. brown dwarfs; hereafter BD) on the dynamics and orbital stability of the inner planets has been highlighted. This has led to constant efforts to identify outer companions for those stars hosting planets plus long term RV drifts.

Gl 86 A is a K0V star with an estimated mass of $0.8\,M_\odot$ (Siess et al. 1997; Baraffe et al. 1998) and is located at 10.9 pc from the Sun (Perryman et al. 1997). Through RV measurements, Queloz et al. (2000) detected a 4 M_J (minimum mass) planet Gl 86 b, orbiting Gl 86 A at ~0.11 AU. This star is also surrounded by a more distant companion Gl 86 B, discovered at ~20 AU using coronography coupled to adaptive optics imaging (Els et al. 2001). The estimated photometry of Gl 86 B is compatible with that expected for a 40–70 M_J brown dwarf companion. However, Mugrauer & Neuhäuser (2005) showed recently that this was also compatible with a cool white dwarf, and that the latter hypothesis was more likely regarding the K band spectrum of the companion. The absence of near-IR molecular and atomic lines as well as the steep K-band continuum are consistent with what is expected for a high gravity object with an effective temperature higher than 4000 K.

Apart from the RV wobble due to the hot Jupiter companion, Gl 86 A also exhibits a long term RV drift measured with CORAVEL and CORALIE over 20 years. This drift indicates the possible presence of an additional more distant companion, with a substellar mass and a distance to star greater than ≃20 AUs. Els et al. (2001) claimed that Gl 86 B cannot account for this RV drift, due to its low mass. They postulated instead that an additional companion, located in 2000 "behind" the star (i.e., under the coronographic mask), could be responsible for the observed drift.

In the course of a deep search for faint outer companions to stars hosting planets with NACO, we were able to make new images of Gl 86 A and B in the near IR. We present the observational results in Sect. 2. In Sect. 3, we report new photometric result of Gl 86 B and we present an analysis of both astrometric and RV data, assuming that the RV drift is due to Gl 86 B. In Sect. 4 we discuss the nature of Gl 86 B, and we confirm that it is very probably a $\sim 0.5\,M_\odot$ white dwarf. We discuss the implications of this hypothesis.

2. Observations

2.1. NACO observing log

Observations of Gl 86 were performed on November 12, 2003, September 22, 2004 and July 29, 2005 with NACO at the VLT. NACO is equipped with an adaptive optics system

* Based on ESO observing programs 70.C-0543, 072.C-0624 and 073.C-0468 at the VLT.

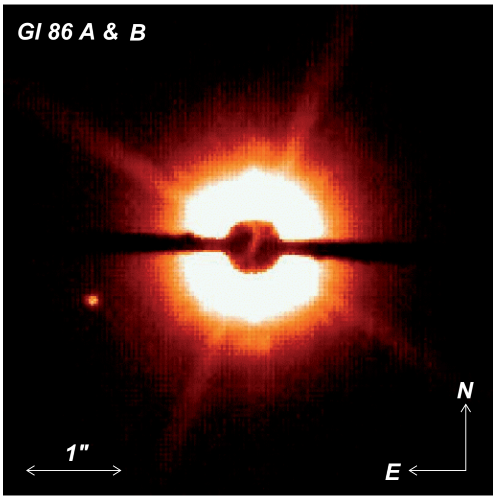

Fig. 1. VLT/NACO K_s-band coronagraphic image of Gl 86 A and B, acquired on September 24, 2004, with an occulting mask of diameter 0.7″.

(Rousset et al. 2002; Lagrange et al. 2002) that provides diffraction limited images in the near infrared (IR) and feeds the observing camera CONICA (Lenzen et al. 2002). Both coronagraphic and direct images were performed to image respectively Gl 86 B and A within the linearity domain of the detector. Note that between the two observing dates, the CONICA detector was changed and the latter detector was more efficient.

The calibrations of platescale and detector orientation were done using the Θ_1 Ori C astrometric field on November 12, 2003, September 22, 2004 and July 29, 2005. On November 12, 2003 and July 29, 2005, the orientation of true north of the S27 camera was found respectively at −0.06° and −0.05° east of the vertical with an uncertainty of 0.20° and the platescale was 27.01 ± 0.10 mas. On September 22, 2004, the orientation of true north of the S13 camera was found 0.20° east of the vertical with an uncertainty of 0.20° and the platescale was 13.25 ± 0.10 mas. Table 1 summarizes the new observations as well as archival ones and Fig. 1 shows a K_s ($\lambda_c = 2.2\,\mu$m, $\Delta_\lambda = 0.35\,\mu$m) image recorded in September 2004.

2.2. Photometric measurements

On July 29, 2005, the NACO measurements of Gl86 A and B were obtained in J, H and K_s filters, under photometric conditions. The JHK_s contrasts were determined using the deconvolution algorithm of Véran & Rigaut (1998). Based on the JHK photometry of Gl86 A from the 2MASS All-Sky Catalog (Cutri et al. 2003), we then deduced the JHK photometry of Gl86 B (see Table 1). The transformation between the K_s filter of NACO and the K filter used by CTIO-2MASS was found to be smaller than 0.03 mag.

The reported photometry is significantly different from the ones given by Els et al. (2001) (see Table 1). This could be related to systematic photometric errors induced by an incorrect subtraction of the Gl 86 A PSF wings within the coronagraphic image. This effect is generally larger for shorter wavelengths where AO corrections are poorer. It often leads to an underestimation of the companion flux, as is the case in Table 1 when comparing ADONIS and NACO data. Thanks to the highest angular resolution and the enhanced detection capabilities provided by NACO at VLT, we can reasonably expect our data to be less sensitive to this PSF subtraction effect in deriving the Gl 86 B photometry.

The new NACO photometry is still compatible with the conclusions of Els et al. (2001) that Gl86 B has a photometry similar to that expected for a substellar companion with a mass of 40–70 M_J (spectral type L7–T5). However, this photometry can also correspond to the one expected for a cool white dwarf and, as recently claimed by Mugrauer & Neuhäuser (2005), this is more likely the case as the spectrum of Gl 86 B does not exhibit the molecular absorption features in K band that are characteristic of L or T dwarfs.

In the following, we reinvestigate this issue (brown or white dwarf) from a dynamical point of view.

2.3. Astrometric measurements

The offset positions of Gl 86 B to A, recorded with NACO on 12 November 2003, 22 September 2004 and 29 July 2005, were translated into physical values using the corresponding astrometric calibration data. The shifts induced by the use of different filters between coronographic and direct images were taken into account. Table 3 summarizes the measured values and Fig. 2 shows the various data points in a ($\Delta\alpha$, $\Delta\delta$) diagram, as well as the offset positions of Gl 86 B to A measured by (Els et al. 2001) with ADONIS/SHARPII on 8 September 2000. The orbital motion of Gl 86 B is clearly identified. This confirms the independent detection of Mugrauer & Neuhäuser (2005).

2.4. Radial velocity data

Radial velocity measurements of Gl 86 A have been gathered for more than 20 years. The whole data set reveals, in addition to a short period modulation of ~1 km s^{-1} amplitude that has been attributed to a hot Jupiter companion (Queloz et al. 2000), the presence of a regular continuous decrease of ~2 km s^{-1} in 25 years (Fig. 7).

It is tempting to try to attribute this regular decrease to Gl 86 B. The temporal derivative of the radial velocity of the primary in a binary system is easy to derive. One gets

$$\frac{\mathrm{d}v_r}{\mathrm{d}t} = -\frac{Gm}{r^2}\sin i \sin(\omega + v) \quad (1)$$

where G is the gravitational constant, m is the mass of the companion r is the distance between the two bodies, i is the inclination of the orbit with respect to the plane of the sky, ω is the argument of periastron, and v is the true anomaly, i.e. the current polar position along the orbit with respect to the periastron. Of course most of these quantities are unknown, but a simple application assuming $\sin i \sin(\omega + v) \simeq 0.5$ and $r \simeq 20$ AU shows that $\mathrm{d}v_r/\mathrm{d}t \simeq -2$ km s^{-1}/25 yr is hardly compatible with $m = 70\,M_J$, but rather with m ranging between 0.2 and 1 $M_\odot$.

This result led Els et al. (2001) to conclude that the RV residuals are not due to Gl 86 B, but rather to an unseen, additional body. Conversely if we keep attributing the RV decrease to Gl 86 B, this raises the question of the mass of Gl 86 B. The available photometry is compatible with a 70 M_J object (Els et al. 2001). But it can also be compatible with a ~0.5 $M_\odot$ object if this object is a white dwarf. Obviously, more data, in particular spectroscopic data are needed to discriminate between these two possibilities.

Table 1. Observation log. ND_{short} is a CONICA neutral density filter with a transmission of 1.4%. S13 and S27 are two CONICA cameras corresponding respectively to a platescale of 13.25 and 27.01 mas. WFS corresponds to the wave front sensor of the adaptive optics system.

UT Date	Filter	Camera	Observation type	Exp. Time (s)	WFS	Obs-Program	Platescale calibrator
12/11/2003	K_s	S27	coronagraphy (0.7″)	100×0.6	VIS	072.C-0624	Θ_1 Ori C
12/11/2003	2.17 + ND_{short}	S27	direct	15×4.0	VIS	072.C-0624	Θ_1 Ori C
22/09/2004	H	S13	coronagraphy (0.7″)	48×1.0	VIS	073.C-0468	Θ_1 Ori C
22/09/2004	H + ND_{short}	S13	direct	42×0.35	VIS	073.C-0468	Θ_1 Ori C
29/07/2005	K_s	S27	coronagraphy (0.7″)	400×0.8	VIS	075.C-0813	Θ_1 Ori C
29/07/2005	K_s+ ND_{short}	S27	direct	400×0.35	VIS	075.C-0813	Θ_1 Ori C
29/07/2005	H	S13	coronagraphy (0.7″)	$360 \times 1.$	VIS	075.C-0813	Θ_1 Ori C
29/07/2005	H + ND_{short}	S13	direct	400×0.35	VIS	075.C-0813	Θ_1 Ori C
29/07/2005	J	S13	coronagraphy (0.7″)	$165 \times 2.$	VIS	075.C-0813	Θ_1 Ori C
29/07/2005	J + ND_{short}	S13	direct	240×0.5	VIS	075.C-0813	Θ_1 Ori C

Table 2. Photometry of Gl86 A and B.

Component	J (mag)	H (mag)	K (mag)
Gl86 A[a]	4.79 ± 0.03	4.25 ± 0.03	4.13 ± 0.03
Gl86 B[b]	14.7 ± 0.2	14.4 ± 0.2	13.7 ± 0.2
Gl86 B[c]	12.9 ± 0.3	13.1 ± 0.2	12.8 ± 0.2

[a] From the 2MASS All-Sky Catalog (Cutri et al. 2003).
[b] From Els et al. (2001).
[c] From [a] and NACO measurements presented in this work.

Table 3. Offset positions of the Gl 86 B relative to A.

UT Date	Julian Date	$\Delta\alpha$ (mas)	$\Delta\delta$ (mas)	Separation (mas)	Position Angle (°)
08/09/2000	2 451 796	1510 ± 25	−853 ± 6	1734 ± 22	119.5 ± 0.8
10/11/2000	2 451 859	1522 ± 3	−789 ± 20	1714 ± 10	117.4 ± 0.4
12/12/2000	2 551 891	1508 ± 10	−851 ± 13	1732 ± 11	119.4 ± 0.4
12/11/2003	2 452 986	1818 ± 12	−573 ± 4	1906 ± 11	107.5 ± 0.4
22/09/2004	2 453 271	1872 ± 16	−513 ± 6	1941 ± 14	105.3 ± 0.5
29/07/2005	2 453 581	1920 ± 13	−435 ± 9	1969 ± 11	102.7 ± 0.4

3. Data analysis

3.1. General analysis of astrometric data

From Fig. 2, one can see that on the plane of the sky, the four points (see plots below) are roughly aligned, so that the only relevant information we can derive from these data is a middle astrometric position (at $t = 2003.126$) and temporal derivatives of the right ascension α and of the declination δ. We thus perform a least-square fit of the available data to derive them. The result is shown in Fig. 2. We see that α and δ actually vary roughly linearly with time. The linear fit is therefore relevant. The corresponding temporal derivatives are

$$\left\{\begin{array}{l}\dfrac{\mathrm{d}(\alpha)}{\mathrm{d}t} = 89.5 \pm 8.7\ \mathrm{mas\,yr^{-1}} \\ \dfrac{\mathrm{d}(\delta)}{\mathrm{d}t} = 85.6 \pm 7.18\ \mathrm{mas\,yr^{-1}}.\end{array}\right. \quad (2)$$

These derivative values, together with the mean present values of α and δ, provide four contraints on the orbit of the companion with respect to the primary. In principle, this orbit is fully characterized by 6 orbital elements, plus the unknown mass m of the companion. The constraints allow us to fix 4 of them. We chose to let the mass m of the companion, the inclination i with respect to the plane of the sky, and the longitude of the ascending node Ω (with respect to west) as free parameters. For any given set of parameters (m, i, Ω) we are able to derive the remaining ones, i.e. the semi-major axis a, the eccentricity e, the argument of periastron ω and the mean anomaly M. We recall that M is a quantity that characterizes the present position of the companion on its orbit. M is proportional to the time, $M = 0$ at periastron and $M = 2\pi$ one orbital period later.

3.2. Analysis assuming that Gl 86 B is a 70 M_J object

Depending on the free parameter set we choose, there is not necessarily an orbital solution compatible with the constraints. In particular, it turns out that there is no solution for $i < 120°$. This means that we are viewing the orbit nearly from its south pole. The result of the parameter space exploration is shown in Figs. 3–5. The semi-major axis, the eccentricity, and the mean anomaly are plotted as a function of Ω, for different values of the inclination i, and for a fixed companion mass $m = 70\,M_J$. We note that in some cases ($i = 120°$) there is not a solution for every Ω value. We note also that the orbit is necessarily eccentric ($e > 0.35$ in any case), and that in all cases, the companion is at present shortly after periastron ($0 < m < 60°$). Of course we explored other companion masses in the compatible range ($60\,M_J \lesssim m \lesssim 90\,M_J$). The result is not shown here but it is nearly equivalent to that for $m = 70\,M_J$. Figures 3–5 represent the standard solution.

In order to better show the shape of the orbital solution, we display one typical solution, marked as a bullet in Figs. 3–5, and charaterized by $i = 150°$, and

$$\left\{\begin{array}{l}a = 47.58\ \mathrm{AU}\,, \quad e = 0.6185\,, \quad \Omega = 300°, \\ \omega = 19.71°\,, \quad M = 18.58°.\end{array}\right. \quad (3)$$

The projection of this solution onto the plane of the sky is shown in Fig. 6. We clearly see that the orbit is eccentric and that the present day position of the companion is shortly after periastron. The associated orbital period is 353 yr, and the last periastron passage occurred in 1984. Of course the latter quantities are subject to some variations if we consider another solution.

In Fig. 7, we show the Gl 86 radial velocity data set, superimposed on the theoretical curve that would be expected for the solutions we display in Fig. 6. Note that in those curves, we do not add the short period modulation due to the hot Jupiter companion, as this object produces a much smaller amplitude.

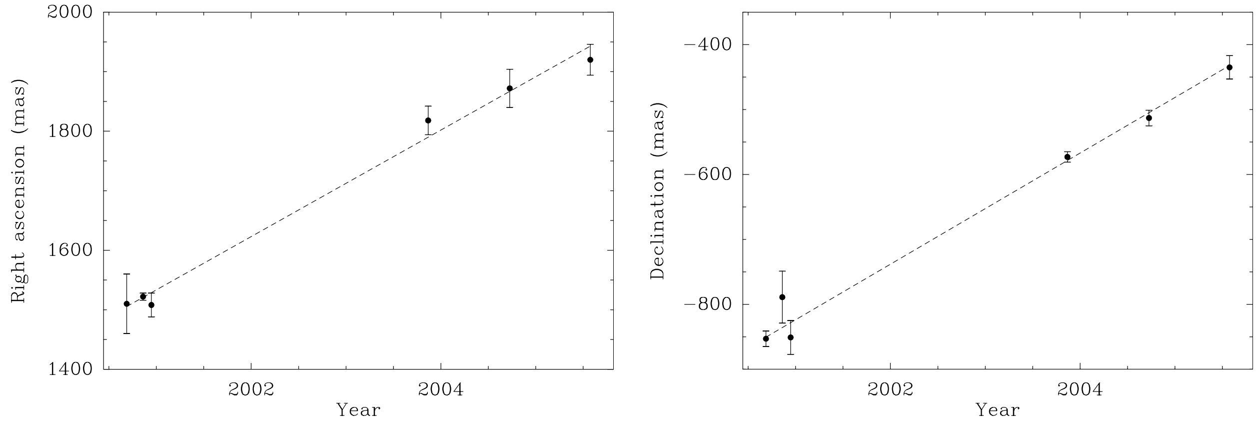

Fig. 2. Least square fits of the right ascension (*left*) and of the declination (*right*) of Gl 86 B relative to A.

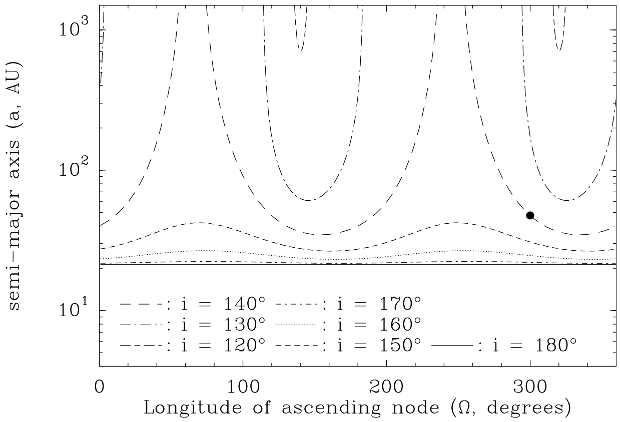

Fig. 3. The semi-major axis a of the orbital solution for the Gl 86 companion, as a function of the longitude of the ascending node Ω, for various values of the inclination i between 120° and 180°, for a fixed companion mass $m = 70\,M_J$. The bullet represents the solution plotted in Fig. 6 (upper plot) and detailed in Eq. (3).

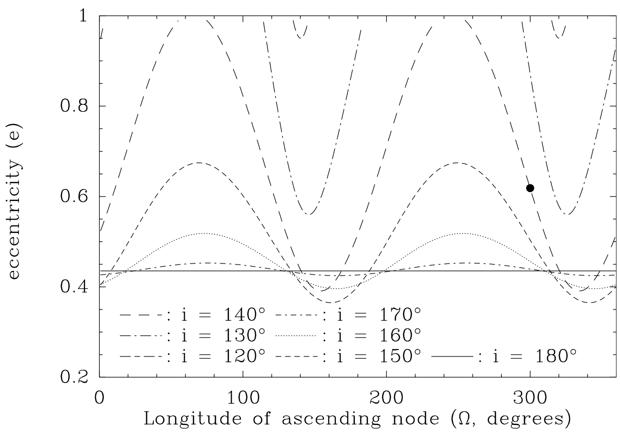

Fig. 4. Same as Fig. 3, but for the orbital eccentricty of the solution.

We also add to the theoretical radial velocity curve an empirical offset, intended to correspond to the mean heliocentric velocity of the Gl 86 system, fixed in such a way that the radial velocity matches the mean observed value in 2003.126. The only relevant parameter we need to compare between the data and the theory is the mean temporal derivative of the radial velocity at in 2003.126, and also the general trend over 25 years.

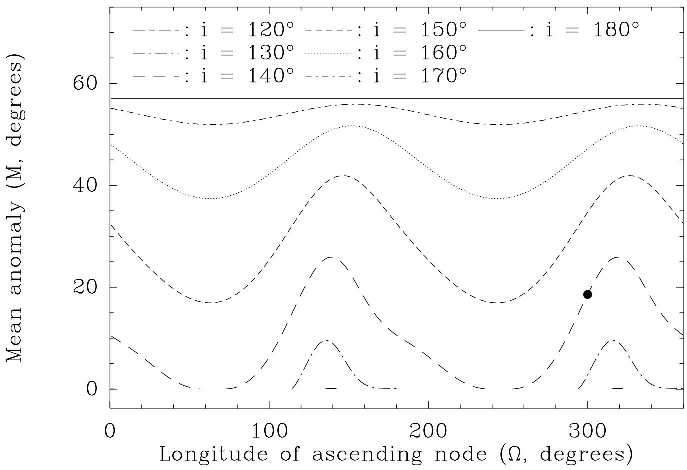

Fig. 5. Same as Fig. 3, but for the present mean anomaly M.

In Fig. 7, the theoretical radial velocity curve corresponding to Eq. (3) is represented as a dashed line. We see that it does not match the data. In fact the decrease in 2003.126 is only 10% of the observed values (0.1 km s^{-1}/25 years). As explained above, this was expected from our order of magnitude estimate of the mass needed to account for the observe decrease rate.

3.3. Analysis assuming Gl 86 B is a ∼0.5 $M_\odot$ object

If we now assume that the residuals of the radial velocity data are due to Gl 86 B, we obtain additional constraints to the orbital parameters. In particular, we can force the temporal derivative of the radial velocity in 2003.126 to match the observed one. This in turn enables us to fix the mass m of the companion instead of giving it as an input parameter. However, this single criterion turned out not to be sufficient. We may derive solutions that fit the radial velocity derivative in 2003.126 but that do not fit the radial velocity data over the whole observation period, especially the older data. Hence we retain in the fitted solutions only those that fit a convenient least square criterion with the whole radial velocity data sample.

The result of the exploration of the parameter space is shown in Figs. 8–11. Note that contrary to Figs. 3–5, solutions are plotted only for $-83° < \Omega < 10°$; there is no convenient solution out of this range of Ω. We see also that there are solutions for $110° < i < 150°$. The orbit is still viewed from the south but it does not exactly lie in the plane of the sky ($i = 180°$). With

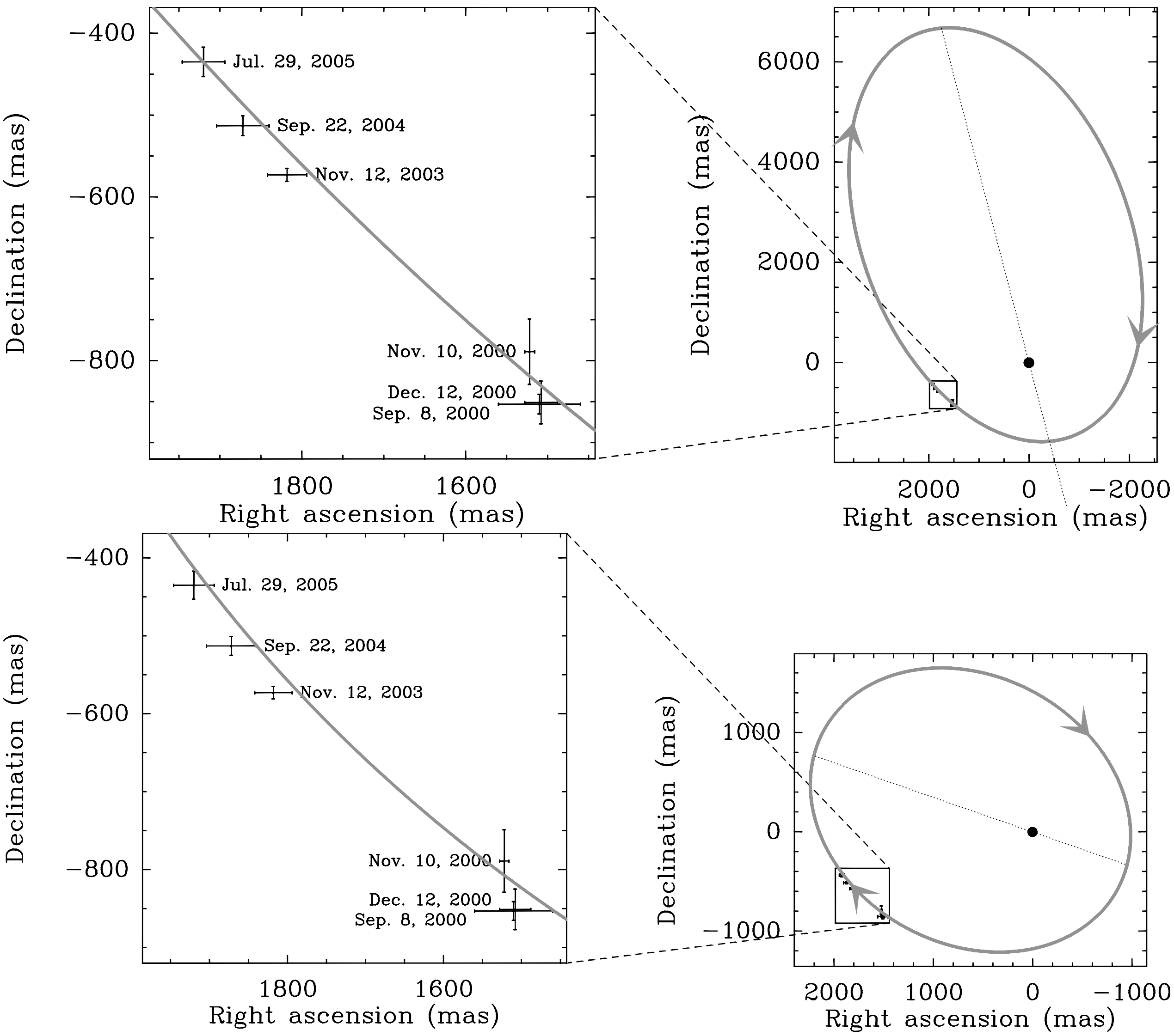

Fig. 6. A representation of the orbital solutions described by Eq. (3) (upper plot, brown dwarf case) and Eq. (4) (lower plot, white dwarf case), as projected onto the plane of the sky. In each case, the right plot represents a view of the full orbit and the left plot is an enlargement of the present day motion. The dotted line is the projection of the line of apsides of the orbit.

exactly $i = 180°$, there would be no radial velocity signature. The significant decrease of the radial velocity as observed over 25 years forces the inclination i not to be too close to $i = 180°$. The solutions are still eccentric, and the present location of Gl 86 B is still more or less soon after periastron. The most interesting outcome concerns the now fitted mass of the companion (Fig. 11). No solution with $m \leq 0.4\,M_{\odot}$ is found, and the more likely solutions correspond to $0.4\,M_{\odot} < m < 0.6\,M_{\odot}$. This is of course very different from typical brown dwarf values, but falls in the range of typical white dwarf masses.

As in the previous section, we display one peculiar solution assumed to represent a standard solution, charaterized by $i = 150°$ and

$$\left\{ \begin{array}{lll} a = 18.42\,\mathrm{AU}, & e = 0.3974, & \Omega = -35°, \\ \omega = -18.05°, & M = 100.5°, & m = 0.4849\,M_{\odot}. \end{array} \right. \quad (4)$$

This solution is marked as a bullet in Figs. 8–11. The orbital period now only 69.7 yr, and the last periastron passage occurred in 1983.

In Fig. 6, we show the projection of this solution onto the plane of the sky as for the orbit corresponding to Eq. (3), and in Fig. 7 we show the corresponding radial velocity curve as a solid grey curve. The agreement with both the radial velocity and the astrometric data is very good. Apart from small changes in the orbital elements, the main difference to the orbit described in Eq. (3) is the mass of the companion. With $m = 0.5\,M_{\odot}$, it is obviously not a brown dwarf.

4. Discussion

4.1. The nature of Gl 86 B

From the above analysis, either Gl 86 B is a brown dwarf, and then it is unable to explain the RV residuals, or it is a ~$0.5\,M_{\odot}$ white dwarf. In the former case, another massive object is required to explain the RV residuals. In that case, one should wonder why this object has not been detected yet, unless it is angularly close to the primary, so that it should disappear under the coronographic mask used in the images, as suggested by Els et al. (2001). Given the inclination we derive for Gl 86 B, the whole system is thus far from being planar. Independent of the low probability that such an additional massive component

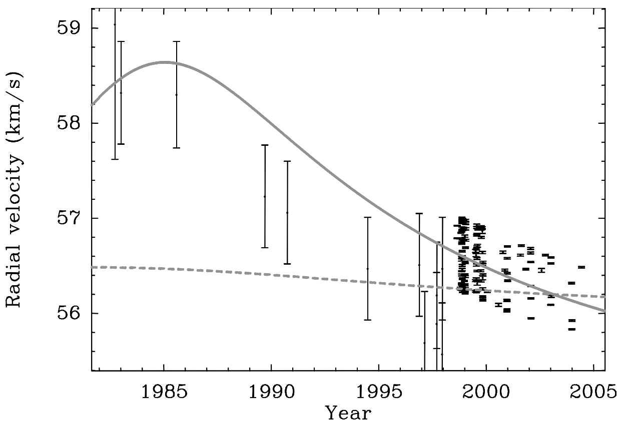

Fig. 7. Radial velocity data of Gl 86 A as monitored over 25 years, superimposed on the theoretical curves (in grey) corresponding to the orbital solutions displayed in Fig. 6. The low accuracy data up to 1998 are the CORAVEL data (typical error ±0.27 km s^{-1}), while the subsequent high accuracy data are the CORALIE ones (typical error ±0.005 km s^{-1}). The dashed curve corresponds to the orbit detailed in Eq. (3) where Gl 86 B is taken as a brown dwarf. The solid curve corresponds to the orbit described in Eq. (4), where Gl 86 B is fitted as a white dwarf. The fit of the radial velocity residuals is much better.

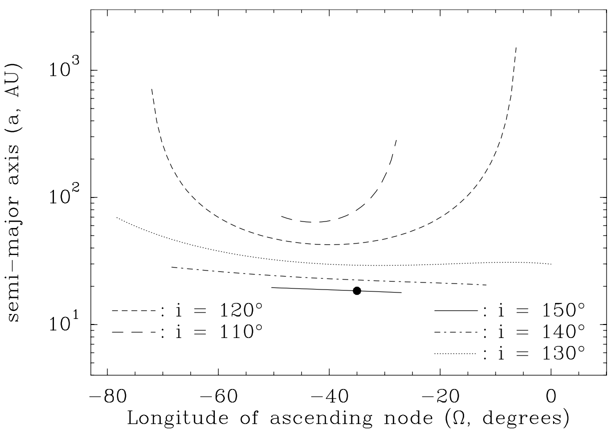

Fig. 8. The semi-major axis *a* of the orbital solution for Gl 86 B that also fits the radial velocity data residuals, as a function of the longitude of the ascending node Ω, for various values of the inclination *i* between 110° and 150°. The bullet represents the solution plotted in Fig. 6 (lower plot), described in Eq. (4).

would be located currently in such a position that it could not be detected, the dynamical stability of the whole system should be questioned. It is well known (Beust et al. 1997; Beust 2003; Krymolowski & Mazeh 1999) that multiple systems with high mutual inclinations are often subject to the Kozai resonance, and that this can lead to instability.

It seems thus more natural to attribute the RV residuals to the sole Gl 86 B companion. In that case, it must be a 0.4–0.6 $M_{\odot}$ object. As from its photometry it cannot be a main sequence star of that mass, Gl 86 B is necessarily a white dwarf. Our dynamical analysis finally leads to the same conclusion that Mugrauer & Neuhäuser (2005) derived from independent spectrophotometric arguments.

Based on the present constraint put on the mass of Gl 86 B and on the new NACO *JHK*s photometry, presented in Sect. 2.2, we can now re-investigate the physical properties of this white dwarf companion, using predictions of the evolutionary cooling sequences models of Bergeron et al. (2001) for hydrogen- and helium-rich white dwarfs.

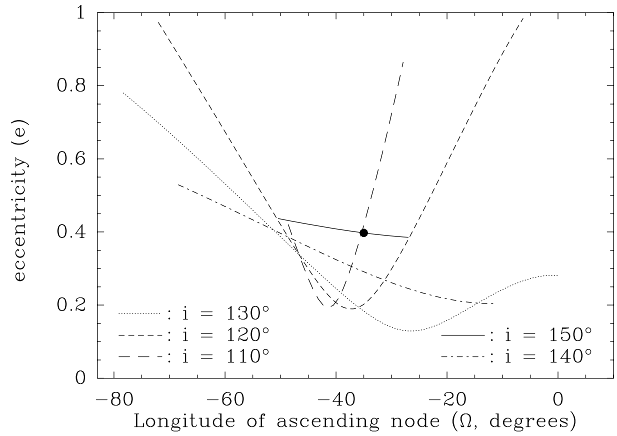

Fig. 9. Same as Fig. 8, but for the orbital eccentricty of the solution.

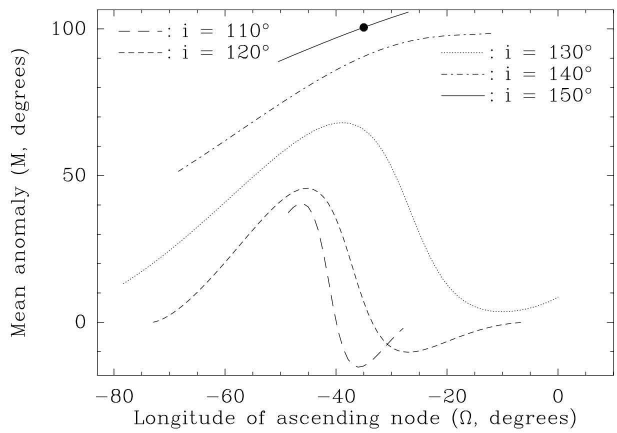

Fig. 10. Same as Fig. 8, but for the present mean anomaly *M*.

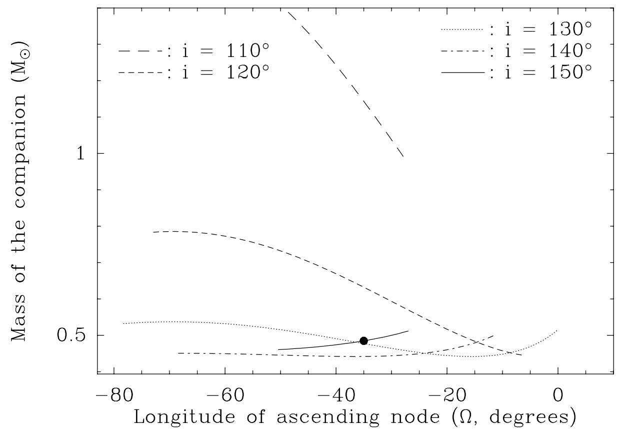

Fig. 11. Same as Fig. 8, but for the fitted mass of the Gl 86 B companion.

The model predictions are reported in a color-magnitude diagram ($J - K$ vs. M_K) for both cases: hydrogen-rich (Fig. 12, *left*) and helium-rich (Fig. 12, *right*) white dwarfs. We notice the discrepancy between the model predictions and the previous photometric data of Els et al. (2001) that Mugrauer & Neuhäuser (2005) used to derive an effective temperature of 5000 ± 500 K for Gl 86 B. Our new NACO photometric data are in very good agreement with the model and with the dynamical constraints. Then, if we add the fact that the mass of Gl 86 B is dynamically constrained between (0.4–0.6 $M_{\odot}$), we can derive the effective temperature, the gravity as well as the cooling age of the Gl 86 B

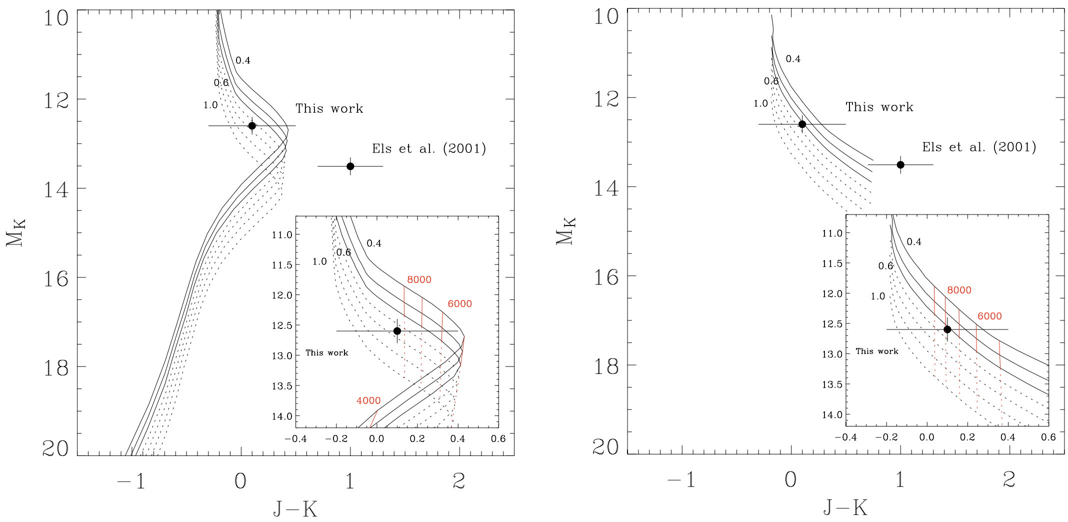

Fig. 12. Color-magnitude diagram ($J-K$ vs. M_K) with model predictions for different masses in two different cases: white dwarfs with hydrogen-rich (Fig. 12, *left*) and helium-rich (Fig. 12, *right*) atmospheres. The predictions for a 0.4, 0.5 and 0.6 $M_\odot$ white dwarf, which is likely the case for Gl 86 B based on our dynamical analysis, are given in *solid lines*, the others in *dotted lines*. The iso-$T_{\rm eff}$ lines (*red*) have been also reported in the zoom-in images. The photometric data from Els et al. (2001) and this work have been reported in both figures for direct comparison with model predictions.

Table 4. Physical parameters of Gl 86 B based on predictions of the evolutionary cooling sequences models of Bergeron et al. (2001) for hydrogen- and helium-rich white dwarfs.

Model	Mass ($M_\odot$)	$T_{\rm eff}$ (K)	log (g)	Cooling age (Gyr)
H-rich	0.4	5500 ± 1000	7.66 ± 0.02	$1.4^{+1.4}_{-0.42}$
	0.5	6000 ± 1000	7.86 ± 0.01	$1.8^{+1.4}_{-0.6}$
	0.6	7000 ± 1000	8.01 ± 0.01	$1.5^{+0.9}_{-0.4}$
He-rich	0.4	6000 ± 1000	7.70 ± 0.01	$1.6^{+1.5}_{-0.6}$
	0.5	7000 ± 1000	7.88 ± 0.01	$1.3^{+0.7}_{-0.34}$
	0.6	8000 ± 1000	8.03 ± 0.01	$1.2^{+0.6}_{-0.29}$

companion based on model predictions. The derived physical parameters for hydrogen- and helium-rich white dwarf model predictions are reported in Table 4.

4.2. The initial-final mass relationship

Both dynamical and spectrophotometric studies come to the conclusion that Gl 86 B is a white dwarf. Let us now investigate the dynamical implications of this hypothesis. The main uncertainty concerns the initial main-sequence mass of Gl 86 B before its evolution to the white dwarf state. This general problem is known as the Initial-Final Mass Relationship (IFMR) for white dwarfs (Jeffries 1997). This problem, together with the upper mass limit for white dwarf progenitors, has been the subject of intense investigations in the past (Weidemann 1977, 1987, 1990).

For Gl 86, a first constraint is that Gl 86 B must have been *more massive* than Gl 86 A in the past (i.e., 0.8 $M_\odot$), in order to have more quickly evolved to the post main-sequence state.

The IFMR is an increasing function of the initial mass. It is usually measured using white dwarfs that are members of open clusters of known ages. Weidemann (1987) gives a semi-empirical IFMR, but further measurements of white dwarfs in NGC 2516 (Jeffries 1997) have shown it was inaccurate. More relevant relations for various metallicities (Z) are given by Hurley et al. (2000). In the following, we will assume the IFMR given by Hurley et al. (2000) (Fig. 18) for $Z = 0.02$.

Note that this IFMR is different from another one that is sometimes shown (Iben 1991; Bressan et al. 1993; Fagotto et al. 1994), which shows the mass of the white dwarf remnant as a function of that of the core at the beginning of the TP-AGB phase. We are interested in the full initial mass of Gl 86 B at Zero Age Main Sequence (ZAMS), so that the first IFMR is relevant here.

4.3. Mass loss in a binary system

Additional constraints can be derived if we consider the past evolution of the mutual orbit of Gl 86 A and B. The important post main-sequence mass loss of Gl 86 B that led to its white dwarf state induced an evolution of the orbit that can be estimated. The general problem of orbital evolution due to mass loss in a binary system has been theoretically investigated by many authors. One must distinguish between slow and rapid mass loss. In the former case, the semi-major axis appears to grow during the mass loss process, while the eccentricity remains secularly unchanged (Jeans 1928; Hadjidemetriou 1963; Verhulst 1972); in the latter case (rapid mass loss) both the semi-major axis and the eccentricity grow (Blaauw 1961; Hut & Verhulst 1981). A major difference is that in the case of slow mass loss, the orbit always remains bound (it just widens), while in the latter case it can be disrupted. This actually occurs if the mass loss exceeds half of the mass of the whole system (Blaauw 1961). This case corresponds typically to supernovae.

In the case of Gl 86, we are concerned by the slow mass loss case. The equations defining the variation of the semi-major axis a and of the eccentricity e are given by Hadjidemetriou (1963):

$$\frac{{\rm d}e}{{\rm d}t} = -\left(e + \cos f\right)\,\frac{\dot{M}}{M}; \qquad (5)$$

$$aGM\left(1-e^2\right) = \text{constant}, \qquad (6)$$

where M is the total mass of the system, $\dot{M}$ the mass loss rate (due here to Gl 86 B only) and f is the true anomaly along the orbit. The second equation arises from the fact that the specific angular momentum $\boldsymbol{C} = \boldsymbol{r} \wedge \boldsymbol{v}$ is unchanged. The first one is derived assuming that the change of the specific orbital energy U is only due to the the mass loss ($\mathrm{d}U/\mathrm{d}t = -G\dot{M}/r$) where r is the radius vector (Verhulst 1974).

If the mass loss is a slow process, Eq. (5) can be averaged over one orbital period. This gives $\overline{\mathrm{d}e/\mathrm{d}t} = 0$, which means that the eccentricity is secularly constant (Jeans 1928; Hadjidemetriou 1963). Subsequently, the evolution of the semi-major axis obeys the simple rule aM = constant. As M decreases, it is obvious that the orbit gets wider. If the total change of M (only due to Gl 86 B) is known from the IFMR, it is then possible to derive the initial semi-major axis.

4.4. Application to Gl 86 A and B

If we apply this theory to the case of Gl 86 B, we are able to derive the former characteristics of the Gl 86 system. The fit of Sect. 3.3 allows to derive the present day orbital and mass characteristics of Gl 86 B (a, e and m). For each solution, using the IFMR of Hurley et al. (2000), we are able to derive the initial mass m_{init}, and subsequently the initial initial semi-major axis a_{init} of the orbit, using aM = constant. All solutions that lead to unreaslistic (negative) values for a_{init} are then eliminated; we also eliminate all solutions for which $m_{\mathrm{init}} < 0.8\,M_{\odot}$, as Gl 86 B must have been initially more massive than Gl 86 A. This can be done for each solution that fits the radial velocity and the astrometric data. This constraint turns out to be by far the strongest one.

The result is shown in Figs. 13–14. In these figures, we plot the resulting values of a_{init}, and m_{init} for all the solutions displayed in Figs. 8–11. However, we only retain those solutions that lead to compatible values for a_{init}, and to $m_{\mathrm{init}} > 0.8\,M_{\odot}$. This is the reason why the curves are often interrupted. In particular, all solutions with $i = 110°$ have been eliminated.

In all cases we have $a_{\mathrm{init}} < a$ (typically $a_{\mathrm{init}} \simeq 0.5a$), showing that the orbit is more detached presently than it was in the past. This is for instance the case for the solution described in Eq. (4), for which we have

$$a_{\mathrm{init}} = 12.97\ \mathrm{AU}\,, \qquad m_{\mathrm{init}} = 0.865\,M_{\odot}. \tag{7}$$

This solution is marked as bullets in Figs. 13–14. We see that a_{init} is not very strongly constrained. The original mass of Gl 86 B is better constrained. In Fig. 14, we see that it may range between 0.8 and 2 $M_{\odot}$, but more probably it was <1.5 $M_{\odot}$. The solutions giving $m_{\mathrm{init}} \simeq 2\,M_{\odot}$ are those that correspond to the smallest values for a_{init} (see Figs. 13, 14). If a_{init} was too small, the past orbital stability of the exoplanet companion of Gl 86 A may be questioned. Obviously this dynamical issue needs to be investigated in further detail. But as a first attempt, let us consider a possible original configuration of Gl 86 with a 0.8 $M_{\odot}$ Gl 86 A and a 2 $M_{\odot}$ Gl 86 B progenitor. The Hill radius around Gl 86 A can thus be estimated to ~0.45 d, if d is the separation between the two stars. If we take for d the periastron of the orbit, with $e \simeq 0.3$ (this is the value derived for such solutions; see Fig. 9), and if we assume that the Hill radius must be at least ~2 times larger than the 0.11 AU semi-major axis of the planet to ensure stability, we derive $a_{\mathrm{init}} \gtrsim 0.7$ AU; actually for all solutions with $a_{\mathrm{init}} < 1$ AU, the orbital stability of the exoplanet is subject to caution.

Another puzzling issue is the way the exoplanet formed. To what extent was the initial circumstellar disk of Gl 86 A that gave birth to its companion truncated by tidal interaction with Gl 86 B? According to Eggenberger et al. (2004), the minimum separation in a binary that allows a large enough circumstellar disk for planet formation to survive ranges between 10 and 50 AU. This could mean that we should remove all solutions with $a_{\mathrm{init}} < 10$ AU, which would result in $m_{\mathrm{init}} < 1.3\,M_{\odot}$.

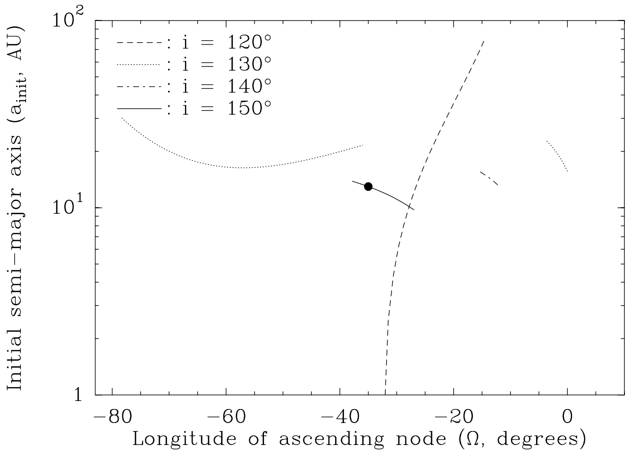

Fig. 13. The initial ZAMS semi-major axis a_{init} of the Gl 86 B as computed for all solutions displayed in Figs. 8–11, using the IFMR from Hurley et al. (2000) and Ma = constant. Only the solutions that fit all the constraints have been retained (see text).

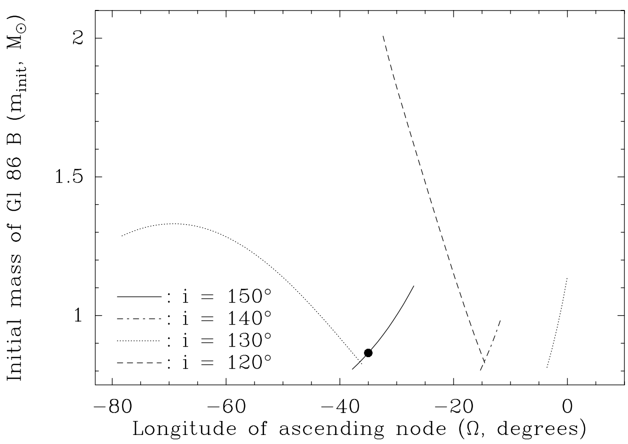

Fig. 14. Same as Fig. 13, but for the initial main-sequence mass of the Gl 86 B progenitor, assuming Gl 86 B is presently a white dwarf.

The constraints on a_{init} and m_{init} help to eliminate some of the fitted solutions in Figs. 8–11. This does not change the basic constraints on a, e and M, but refines that on the present mass m of Gl 86 B. In Fig. 15, we show the same plot as in Fig. 11, but all solutions that do not fulfill the constraints on a_{init}, e_{init} and m_{init} have been removed. In order to explore all possilities, we performed the same calculation for many inclination values (not only for $i = 120°$, $i = 130°$...). The resulting possibilities are summarized as grey areas in Fig. 15. We see that m is fairly well constrained. It is thus possible to state that

$$0.48\,M_{\odot} \leq m \leq 0.62\,M_{\odot} \tag{8}$$

and even probably we could say that $m \leq 0.55\,M_{\odot}$. The sharp lower limit at $m = 0.48\,M_{\odot}$ is due to the lower limit of 0.8 $M_{\odot}$ for m_{init}; the upper limit at $m \simeq 0.61\,M_{\odot}$ corresponds to $a_{\mathrm{init}} = 0$.

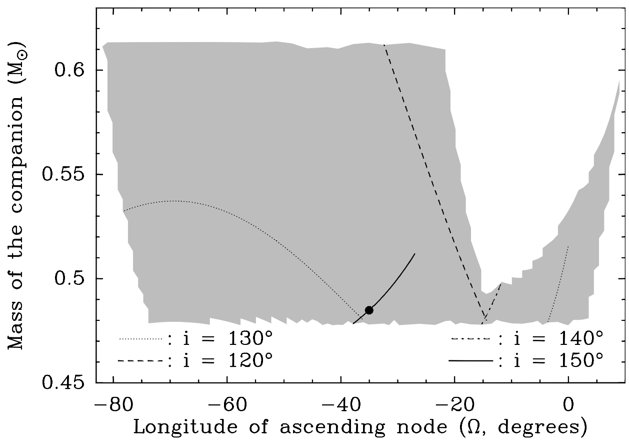

Fig. 15. Same plot as Fig. 11, but all solutions laeding to unphysical or unacceptable values for $a_{\rm init}$ $e_{\rm init}$ or $m_{\rm init}$ have been removed. The grey shaded area corresponds to all possible values if we let the inclination i vary.

5. Conclusion

The identification of the orbital motion of Gl 86 B around Gl 86 A, combined with the measured residuals of the radial velocity data, allow us to severely constrain the whole Gl 86 system and its past evolution. Our dynamical study shows that Gl 86 B is very probably a white dwarf, in agreement with the conclusions of an independent spectrophotometric study by Mugrauer & Neuhäuser (2005). The brown dwarf hypothesis of Els et al. (2001) can therefore be definitively ruled out.

The mass of Gl 86 B is severely constrained by the dynamics. We derive $0.48\,M_\odot \leq m \leq 0.62\,M_\odot$. The orbit is eccentric ($e > 0.4$) with a semi-major axis of a few tens of AU. The associated orbital period is several hundreds of years at least, and the stars have recently (5–20 years ago) passed at periastron. The orbit is retrograde with respect to the plane of the sky, but does not exactly lie in that plane. We can say that $120° \lesssim i \lesssim 150°$.

Based on new photometric results on Gl 86 B and the dynamical mass constrains, we also re-investigated the physical properties of this white dwarf companion. Using model predictions of Bergeron et al. (2001), we derived the effective temperature, the gravity and the cooling age of Gl 86 B for both hydrogen-rich and helium-rich atmospheres models of white dwarfs.

When Gl 86 B was a main sequence star, its mass probably ranged between $0.8\,M_\odot$ and $1.5\,M_\odot$, which implies a spectral type between K2V and F7V. Its orbit was closer. The strong post-main sequence mass loss caused the orbit to widen. If it had been a more massive star, the initial semi-major axis would have been too small to allow orbital stability for the exoplanet orbiting Gl 86 A.

However Saffe et al. (2005) recently used the chromospheric index and metallicity measurements to estimate the age of all known stars harbouring exoplanets. For Gl 86 A, they derived an age ranging between 2 Gyr and 3 Gyr. Given the main sequence lifetimes and the white dwarf cooling times (Table 4), assuming this age for Gl 86 B would imply that its progenitor had $m_{\rm init} \gtrsim 2\,M_\odot$. This seems to be incompatible with our dynamical constraints. To solve this discrepancy, the dynamical evolution of the whole system, including the exoplanet needs to be investigated in more detail. There are many open questions associated with this issue: the exoplanet must have survived all the late evolution stages of Gl 86 B. If the system is not coplanar, the exoplanet could have been subject to the Kozai resonance in the past. Moreover, the planet must have formed in a large enough circumstellar disk, which implies a minimum initial separation of ∼10 AU. All these issues need to be addressed, and this will be the purpose of forthcoming work.

Acknowledgements. We would like to thank the ESO staff of Paranal-La Silla observatory for helping us in the preparation and the execution of our observations. We aknowledge the valuable contribution of Pierre Bergeron who significantly helped us in the use and the interpretation of the cooling models of white dwarfs. We are particularly grateful for his insightful remarks, as well as for the detailed comments of our anonymous referee. We also acknowledge partial financial support from the *Programmes Nationaux de Planétologie et de Physique Stellaire* (PNP & PNPS), in France.

References

Baraffe, I., Chabrier, G., Allard, F., & Hauschildt, P. H. 1998, A&A, 337, 403
Beust, H. 2003, A&A, 400, 1129
Beust, H., Corporon, P., Siess, L., Forestini, M., & Lagrange, A.-M. 1997, A&A, 320, 478
Bergeron, P., Leggett, S. K., & Ruiz, M. T. 2001, ApJS, 133, 413
Blaauw, A. 1961, Bull. Astron. Inst. Neth., 15, 265
Bressan, A., Fagotto, F., & Bergeron, P. 1993, A&AS, 100, 674
Chauvin, G., Lagrange, A.-M., Dumas, C., et al. 2004, A&A, 425, L29
Cutri, R. M., Skrutskie, M. F., van Dyk, S., et al. 2003, 2MASS, All-Sky Catalog of Point Sources
Eggenberger, P., Udry, S., & Mayor, M. 2004, A&A, 417, 353
Els, S. G., Sterzik, M. F., Marchis, F., et al. 2001, A&A, 370, L1
Fagotto, F., Bressan, A., Bertelli, G., & Chiosi, C. 1994, A&AS, 104, 365
Hadjidemetriou, J. D. 1963, Icarus, 2, 440
Hurley, J. R., Pols, O. R., Tout, C. A. 2000, MNRAS, 315, 543
Hut, P., & Verhulst, F. 1981, A&A, 101, 134
Iben, I. 1991, ApJS, 76, 55
Jeans, J. D. 1928, in Astronomy and Cosmogony (London: Cambridge University Press), 267
Jeffries, R. D. 1997, MNRAS, 288, 585
Krymolowski, Y., & Mazeh, T. 1999, MNRAS, 304, 720
Lagrange, A.-M., Moutou, C., ASP Conf. Ser., 321, 23
Lagrange, A.-M., Mouillet, D., Beuzit, J.-L., et al. 2002, SPIE, in press
Lenzen, R., Hartung, M., Brandner, et al. 2002, SPIE, Vol. 4841
Mugrauer, M., & Neuhäuser, R. 2005, MNRAS, 361, 15
Perryman, M. A. C., Lindegren, L., Kovalevsky, J., et al. 1997, A&A, 323, 49
Queloz, D., Mayor, M., Weber, L., et al. 2000, A&A, 354, 99
Rivera, E. J., Lissauer, J. J., Butler, R. P., et al. 2005, A&AS, 207, #191.03
Rousset, G., Lacombe, F., Puget, P., et al. 2002, SPIE, Vol. 4007
Saffe, C., Gómez, M., & Chavero, C. 2005, A&A, 443, 609
Siess, L., Forestini, M., & Dougados, C. 1997, A&A, 324, 556
Véran, J.-P., & Rigaut, F. 1998, SPIE, 3353, 426
Verhulst, F. 1972, CEMDA, 5, 27
Verhulst, F. 1974, CEMDA, 11, 95
Weidemann, V. 1977, A&A, 59, 411
Weidemann, V. 1987, A&A, 188, 74
Weidemann, V. 1990, ARA&A, 28, 103